pubs.acs.org/Biomac

Article

Electric Field-Induced Polarization Responses of Noncentrosymmetric Crystalline Biopolymers in Different Frequency Regimes – A Case Study on Unidirectionally Aligned β-Chitin Crystals

Inseok Chae, Rui Zu, Amira Barhoumi Meddeb, Yu Ogawa, Zhe Chen, Venkatraman Gopalan, Zoubeida Ounaies, and Seong H. Kim*

Cite This: *Biomacromolecules* 2021, 22, 1901–1909

Read Online

ACCESS | Metrics & More | Article Recommendations | Supporting Information

ABSTRACT: A dielectric medium containing noncentrosymmetric domains can exhibit piezoelectric and second-harmonic generation (SHG) responses when an electric field is applied. Since many crystalline biopolymers have noncentrosymmetric structures, there has been a great deal of interest in exploiting their piezoelectric and SHG responses for electromechanical and electro-optic devices, especially owing to their advantages such as biocompatibility and low density. However, exact mechanisms or origins of such polarization responses of crystalline biopolymers remain elusive due to the convolution of responses from multiple domains with varying degrees of structural disorder or difficulty of ensuring the unidirectional alignment of noncentrosymmetric domains. In this study, we investigate the polarization responses of a noncentrosymmetric crystalline biopolymer, namely, unidirectionally aligned β-chitin crystals interspersed in the amorphous protein matrix, which can be obtained naturally from tubeworm *Lamellibrachia satsuma* (LS) tube. The mechanisms governing polarization responses in different dynamic regimes covering optical (>10^{13} Hz), acoustic/ultrasonic (10^{3}–10^{5} Hz), and low (10^{-2}–10^{2} Hz) frequencies are explained. Relationships between the polarization responses dominant in different frequencies are addressed. Also, electromechanical coupling responses, including piezoelectricity of the LS tube, are quantitatively discussed. The findings of this study can be applicable to other noncentrosymmetric crystalline biopolymers, elucidating their polarization responses.

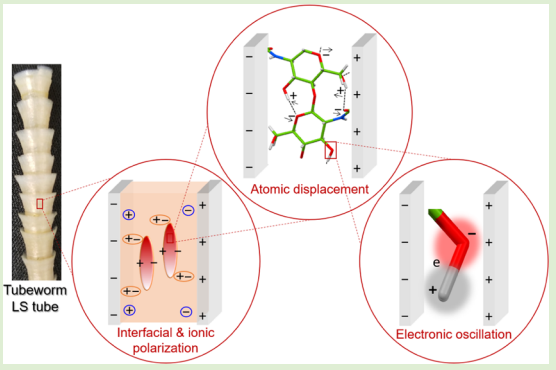

1. INTRODUCTION

Many biopolymers have noncentrosymmetric crystalline structures with asymmetric arrangements of polymer chains.[1−4] When an external electric field is applied, their polarization responses can be manifested as electromechanically coupled strain,[2,5−8] electric polarization,[9−11] nonlinear optical process,[12−14] etc. For example, β-chitin and cellulose Iβ have crystalline structures with 2-fold helices along the chain axis (the *c*-axis of the unit cells), which are packed in parallel (i.e., pointing the same direction).[15−17] Due to the parallel packing and existence of a net dipole in the crystal unit cell, piezoelectricity has been anticipated for materials containing them.[2,10,18−22] The noncentrosymmetric biocrystals are also active in nonlinear optical processes including second-harmonic generation (SHG) and sum-frequency generation (SFG) due to the lack of inversion symmetry.[18,23−29] Other electromechanical coupling responses under an electric field can also appear in both crystalline and noncrystalline domains, which include ion migration, electrostriction, electrostatic effect, and so on.[30,31]

Ascertaining the mechanisms governing polarization responses in biomaterials is essential to suitably exploit their electric field-induced polarization properties. One of the main parameters to consider is the frequency of the applied electric field.[32] Different mechanisms are triggered by the electric field at different frequency regimes, mainly due to limiting characteristic dynamics.[33] Electronic polarization is induced by an electric field in a high-frequency regime up to optical ranges.[32] Atoms and molecules are much heavier than electrons, thus their polarization responses will occur in a lower-frequency regime.[32] Ion migration and space charges are observed in even lower-frequency regimes.[30,32,34] Understanding the polarization mechanisms in different frequency

Received: December 23, 2020
Revised: March 17, 2021
Published: April 2, 2021

https://doi.org/10.1021/acs.biomac.0c01799
Biomacromolecules 2021, 22, 1901–1909

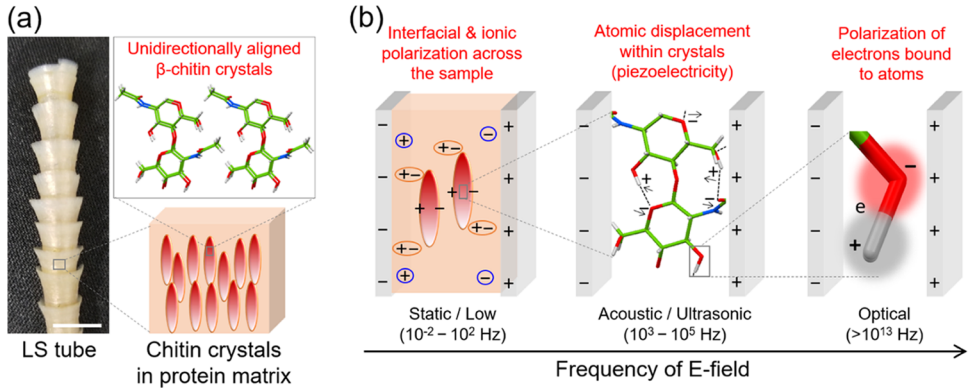

Figure 1. (a) Photographic image of the LS tube and illustrations of the unidirectional alignment of β-chitin crystals. The scale bar represents 1 cm. In the β-chitin chain, green, blue, red, and gray colors represent C, N, O, and H atoms, respectively. (b) Anticipated electric field-induced polarization responses of the LS tube in different frequency regimes. The black arrows in the acoustic/ultrasonic frequency regime represent the anticipated directions of atomic displacements under the electric field.

regimes will elucidate how and why the material responds to applied electric fields in various applications.

Another critical parameter to consider in studying polarization responses of biopolymers is the distribution of physical domains in space.[2,33] The polarization responses depend on the orientation and density of polar domains in the materials. For example, the noncentrosymmetry of the crystal structure anticipates the piezoelectricity of each crystallite, but it can be reduced or canceled on a macroscopic scale when individual crystalline domains are arranged in an antiparallel or random fashion.[2,35,36] On the other hand, the piezoelectric responses can be added when the domains are arranged in a parallel fashion.[2,36] The nonlinear optical processes such as SHG and SFG are also governed by the arrangement of noncentrosymmetric crystallites within the coherence length, which varies from tens of nanometers to the entire bulk sample depending on the optical geometry.[14,24,37,38] Due to the heterogeneous nature of biopolymers, it has been challenging to accurately quantify the polarization responses.[2]

In this study, we investigate how the electric field-induced polarization responses of semicrystalline biopolymers are manifested differently depending on the frequency regimes of the external field. A wide range of frequencies is covered: optical frequencies (>10^{13} Hz), acoustic/ultrasonic frequencies (10^3–10^5 Hz), and low frequencies (10^{-2}–10^2 Hz). *Lamellibrachia satsuma* (LS) was employed since it has a unidirectional arrangement of polar β-chitin crystals in the entire tube.[16] X-ray diffraction analysis found that the LS tube has fibrous β-chitin crystals, namely, microfibrils, interspersed in the amorphous protein matrix with their reducing ends (*c*-axis) of chitin chains pointing up along the long axis of tubes, and the (110) plane is perpendicular to the surface of tubes.[16] Thus, it can be considered a semicrystalline composite containing noncentrosymmetric domains with the same polarity. Figure 1 illustrates the expected electric field-induced responses in the different frequency regimes. In the optical frequency regime, electronic oscillations in atoms can occur under the polarized light and the SHG response is expected due to the noncentrosymmetric crystal structure of β-chitin.[23,38] In the acoustic/ultrasonic frequency regime, the piezoelectric response is expected, as atomic displacements within noncentrosymmetric crystals can occur under the electric field.[10,19] In the low-frequency regime, other electromechanical coupling processes are expected due to the space charge, ion migrations, etc., across the sample.[30,39] We experimentally measured the polarization responses and discussed the dominant polarization mechanisms operating in each frequency regime. The SHG at 800 nm excitation was measured as a representative nonlinear response. Piezoelectric force microscopy (PFM) was used to quantify the piezoelectricity of the unidirectionally aligned β-chitin crystals in the sample in the acoustic frequency regime. Also, dielectric response and electric field-induced strain were measured at frequencies below 100 Hz.

2. EXPERIMENTAL DETAILS

2.1. Preparation of LS Tubes and Wide-Angle X-ray Scattering (WAXS). LS tubeworms were collected from the sea of Kagoshima Bay using a remotely operated vehicle, Hyper-Dolphin (JAMSTEC, Tokyo, Japan). After the collection, the body of tubeworms was separated from tubes by washing with water. The LS tubes were cylindrical, typically 10–20 cm in length and ~7 mm in diameter. The tubes were flattened after cutting the side edges and then dried between two slide glasses at 80 °C under 0.01 MPa overnight. The dried LS tubes were cut in squares with an area of 1–4 cm^2 for different measurements in this study. Two-dimensional (2D) WAXS of the LS tube in a transmission mode was performed using a Xeuss 2.0 HR (Xenocs, France). An X-ray wavelength of 1.54 Å (50 kV, 0.6 mA) and a Pilatus3 R200K detector with a sample-to-detector distance of ~0.165 m were used in the measurement.

2.2. SHG Measurement. The SHG signal was collected for the flat and dried LS tube in transmission geometry with a long axis of the LS tube oriented along the vertical direction (defined as the *y*-axis) and an incident beam normal to the sample plane (defined as *z*-axis). The incident beam was generated with a Ti:Sapphire femtosecond laser system (1 kHz, 80 fs) with the energy centered at 800 nm. The fundamental light passed through a half-waveplate and was focused onto the LS tube. The generated SHG signals were then collected and recorded with a photomultiplier tube with an analyzer placed at the front, parallel (*y*-axis), and perpendicular (*x*-axis) to the chain direction. To obtain the polar plots, the polarization direction of the incident beam was rotated with every 4 ° using the half-waveplate.

2.3. PFM Measurement. Physical deformation/displacement of the flattened LS tube under the AC electric field was measured using a Nanoscope IIIa Multimode atomic force microscope (AFM), equipped with a signal access module (SBOB-1, Digital Instrument), a lock-in amplifier (7260, EG & G instruments), and a high-voltage amplifier (609D-6, Trek). Circular gold electrodes (5 mm in diameter) with a thickness of 100 nm were deposited at the top and bottom surfaces of the flat LS tube using a plasma-sputtering machine (EM150R S, EMS Quorum). To avoid structural artifacts, the LS tube was adhered to a fused quartz substrate using a double-

https://doi.org/10.1021/acs.biomac.0c01799
Biomacromolecules 2021, 22, 1901–1909

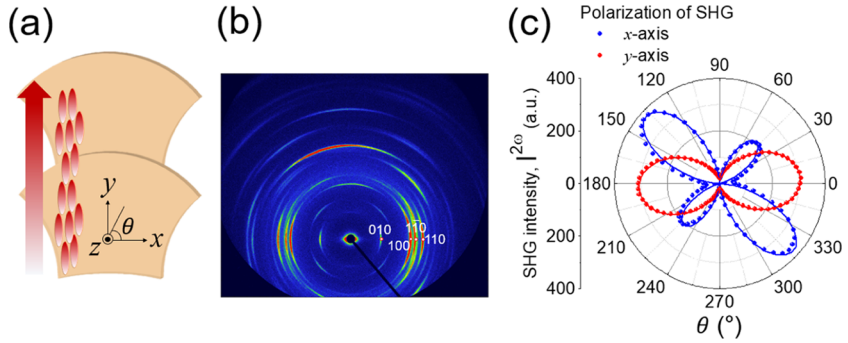

Figure 2. (a) Schematics of the SHG measurement on the flat LS tube with a thickness of ~50 μm. The incident 800 nm beam is aligned along the z-axis and its polarization is rotated within the x−y plane (azimuth angle, θ). (b) 2D WAXS patterns of the LS tube, which confirms the uniaxial alignment of β-chitin chains along the long axis of the LS tube (y-axis). (c) SHG intensities at the polarization of the SHG beam along the y-axis (red color) and the x-axis (blue color) as a function of the polarization angle (θ) of the 800 nm incident beam. The lines are the fit results (details are provided in Section A in the Supporting Information).

sided tape. The AC voltage was generated using the lock-in amplifier and the high-voltage amplifier and then applied to the sample through the bottom electrodes using a copper tape; the top electrode, with which the AFM probe was in contact, was grounded. The frequency of the AC electric bias was scanned as a step function with a 1 kHz/sec rate from 1 to 100 kHz. AFM probe (NCHV-A, Bruker, MA) with a resonance frequency of ~320 kHz and a spring constant of ~40 N/m were used in a contact mode to measure the topography, force error, PFM amplitude, and PFM phase. The same method was used to measure the out-of-plane electromechanical responses of three standard samples for comparisons: (i) poled lead zirconate titanate (PZT) with a thickness of 250 μm, (ii) poled β-poly(vinylidene difluoride) (β-PVDF) with a thickness of 55 μm, and (iii) unpoled poly(vinylidenefluoride-*co*-trifluoroethylene) [P(VDF-TrFE)] 75/25 mol% with a thickness of 15 μm.

2.4. Polarization−Strain−Electric Field and Impedance Spectroscopy. Before the low-frequency tests, 5 mm diameter circular gold electrodes were deposited on both sides of the samples using a plasma-sputtering machine. A modified Sawyer−Tower circuit was used to measure polarization as a function of the electric field. The current was integrated into the charge using a capacitor connected in series with the sample. The sample with Au electrodes was placed between the two pins of the fixture containing the linear variable differential transformer (LVDT). Before applying the electric field, the fixture was submerged in Galden oil, which is insulating and inert, to avoid arcing. The AC electric field at 1 Hz was applied across the thickness of the sample, and then displacement along the field was measured using the LVDT sensor and a Stanford research 830 (SR 830) lock-in amplifier. The impedance spectroscopy measurement was carried out using Modulab XM MTS system.

3. RESULTS AND DISCUSSION

3.1. Optical Frequency Regime (>10^{13} Hz). In the optical frequency regime, a strong SHG signal of the LS tube was measured due to the uniform arrangement of crystalline β-chitin domains inside the tube. SHG is a nonlinear optical process in which a material interacts with two photons with energy $\hbar\omega$ transitioning to a virtual electronic state and emits one photon with energy $2\hbar\omega$ upon relaxation to the ground state.[38] Mathematically, SHG is defined as[38]

$$P_i^{2\omega} = \chi_{ijk} E_j^{\omega} E_k^{\omega} \quad (1)$$

where $P^{2\omega}$, χ_{ijk}, and E^{ω} represent nonlinear polarization of the material, third rank tensor of second-order optical susceptibility, and electric fields induced by the incident light, respectively.[38] Since the frequency of electric fields (ω) is very high, the oscillating dipoles probed by SHG are mainly from the collective polarization of electron clouds.[32] Based on Neumann's principle, the format of the SHG tensor for a β-chitin crystal having the $P2_1$ symmetry is restricted to only eight non-zero tensors (see Section A in the Supporting Information).[16,17,40]

Through the mathematical fitting of SHG polar plots in Figure 2c, the anisotropic arrangement of polar domains in the LS tube was identified. In the transmission geometry, the coherence length of SHG is comparable to the entire sample thickness (~50 μm) (see Figure S2 in the Supporting Information). Thus, the measured SHG signal intensity is the collective response of all crystallites across the entire sample from front to back (z-axis). Two major domains (∥ domain: polar axis parallel to the y-axis and ⊥ domain: polar axis parallel to the x-axis) were employed in the fitting.[41] The phase difference between the two major domains was considered in the SHG fitting (see eqs 3 and 4 in the Supporting Information).[42] The fitting results show that the ∥ fraction is 85−91% and the ⊥ fraction is 9−15%. This confirms that the point group of the LS tube is 2, and the polar axis of the LS tube (2-fold screw axis of β-chitin) is mostly aligned along the long axis of the tube (y-axis).[16] Also, the ratio of χ_{yxx}/χ_{yyy} was found to be ~2 from the fitting, which implies that a larger nonlinear polarization can be induced along the y-axis of the LS tube when the incident electric field is along the x-axis (χ_{yxx}) rather than the y-axis (χ_{yyy}).

The strong SHG response from the β-chitin crystals in the LS tube is consistent with the previous study probing the transition dipole moments of O−H, N−H, and C−H vibration modes of chitin using vibrational SFG spectroscopy in the mid-IR optical frequency regime.[23] The β-chitin crystals generated strong SFG signals because of the parallel packing of chitin chains inside the unit cell.[23] On the other hand, the α-chitin crystals generated much weaker SFG signals due to the antiparallel packing of chains in the unit cell with the orthorhombic symmetry.[23]

3.2. Acoustic/Ultrasonic Frequency Regime (10^3−10^5 Hz). In the acoustic/ultrasonic frequency regime, the unit cell dimension of a noncentrosymmetric biopolymer crystal can be altered under the electric field via collective motions of atoms depending on the orientation of molecular dipoles with respect to the applied field. Their collective displacement under the field is a result of the converse piezoelectricity,[36,40,43] which is described as[43]

https://doi.org/10.1021/acs.biomac.0c01799
Biomacromolecules 2021, 22, 1901−1909

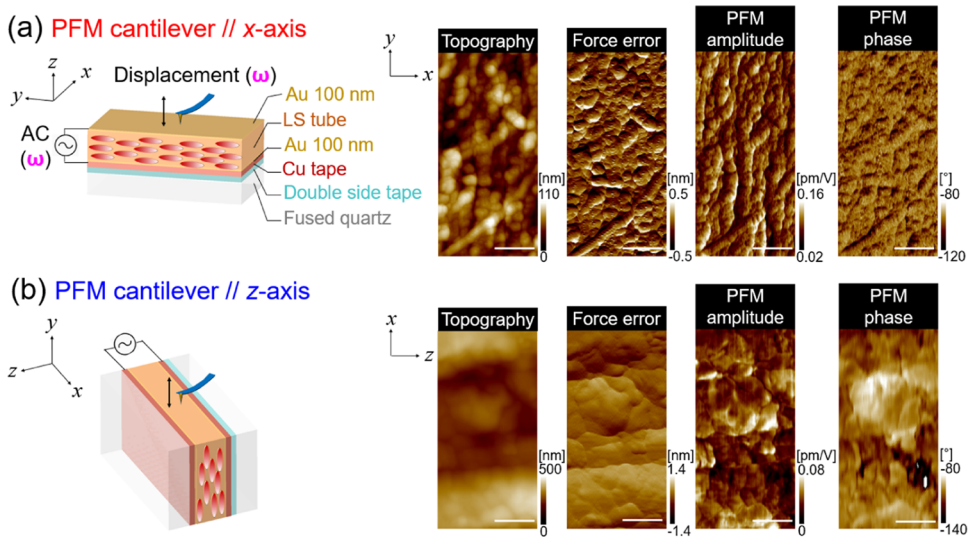

Figure 3. PFM measurements of the flat LS tube in two different geometries: (a) PFM cantilever // the *x-axis* and (b) PFM cantilever // the *z-axis*. The AC electric field of 250 V at 40 kHz was applied through the LS tube (*z*-axis) with a thickness of 100 μm. The scale bars represent 1 μm.

$$S_{ij} = d_{ijk}E_k \quad (2)$$

where S_{ij}, d_{ijk}, and E_k are the induced (electromechanical) strain, piezoelectric coefficient, and applied electric field, respectively.[36] The converse piezoelectricity of the β-chitin crystal is surmised in the LS tube as the noncentrosymmetric crystals are unidirectionally aligned with the polar directionality in the entire tube, as confirmed by the SHG analysis in Section 3.1.

The electromechanical strain of the LS tube under the AC electric field in a 1−100 kHz frequency regime is measured using PFM. It is important to note that the PFM signal is not just due to the piezoelectric response, and other electromechanical coupling responses such as electrostriction, electrostatic effect, and flexoelectricity can also contribute to the PFM signal.[44−47] To unambiguously confirm a piezoelectric response, both direct (polarization induced by stress) and converse coefficients should be measured and then matched, as they are thermodynamically equivalent.[2] However, it is difficult to measure the direct coefficient using PFM since the charging current under cantilever-induced force is expected to be too small to resolve.

To minimize the contribution of other electromechanical effects and obtain quantitative information on the intrinsic piezoelectricity of the LS tube, several control experiments were carried out. We found that orders of magnitude higher PFM responses are measured when there is an air gap between the tube and the bottom solid electrode; such artifacts should be avoided by intimately adhering the sample to the amorphous solid substrate (Section B in the Supporting Information). The LS tube was flattened by applying mechanical pressure and attached to the fused quartz substrate to reduce the contribution from structural artifacts with any air gap to the PFM signal.[44] Also, the AC electric field was applied through the deposited Au electrodes on the top (ground) and bottom (applied voltage) of the tube. This method is better than applying the electrical bias through a conductive PFM cantilever for quantitatively measuring piezoelectric coefficients because the effective electric field on the sample is spatially uniform through the two parallel electrodes coated on the sample over a large area. This is important because the presence of a local field gradient around the PFM probe can also induce flexoelectricity, which may mask a piezoelectric response.[46] The deformation of the LS tube under the electric field was measured using a nonconductive cantilever at the same frequency as the applied electric field (ω). A relatively stiff cantilever (NCHV-A, $k \approx 40$ N/m) was used to minimize the electrostatic artifact due to capacitive coupling between the cantilever and the sample.[44,45]

Considering that the piezoelectricity is an anisotropic material property,[32,36] two different geometries were employed: PFM cantilever along (//) the *x*- and *z*-axes, as shown in Figure 3a,b, respectively. The sample coordination in Figure 2a (the *x*-, *y*-, *z*-axes of the LS tube) was also used in the PFM analysis. In both cases, the AC electric field was applied through the flat LS tube normal to the surface (*z*-axis), and vertical displacements of the PFM cantilever at the same frequency of the applied field were measured while the cantilever is contacting the surface of the LS tube. When the PFM cantilever is parallel to the *x*-axis (Figure 3a), the vertical PFM signal originates from the strain generated along the *z*-axis (perpendicular to the chitin chain axis). There can be an additional contribution from the strain along the *x*-axis due to buckling effects.[48,49] The buckling oscillation occurs when the piezoelectric response from in-plane polarization is aligned along the long axis of the PFM cantilever; the in-plane piezoelectric displacement is coupled in the vertical PFM signal due to the friction between the tip and the sample.[48−50] When the PFM cantilever is parallel to the *z*-axis (Figure 3b), it mainly measures the strain along the *y*-axis (parallel to the chitin chain axis) and the additional displacement from the buckling effects along the *z*-axis.

Relatively small electromechanical responses were measured in the two geometries, as shown in Figure 3. The piezoelectric displacements in two cases are up to 40 and 20 pm at an applied field of 250 V across the sample, which are orders of magnitude higher than the noise level of the system (sub- or few-pm level). Also, the PFM signals are locked with a relatively constant phase (within the 40−60° range) with respect to the applied AC field. Accordingly, the measured signals should be from the actual electromechanical responses of the tube and not an external noise. It is difficult to identify

https://doi.org/10.1021/acs.biomac.0c01799
Biomacromolecules 2021, 22, 1901−1909

how much contribution of the electrostatic effect appears in the measured signals, but we can still conclude that the upper bound of the piezoelectricity of the LS tube in these two geometries is roughly 0.2 pm/V at 40 kHz. Consistently low piezoelectric responses of the LS tube were measured in the 1−100 kHz frequency regime, as shown in Figure 4. The

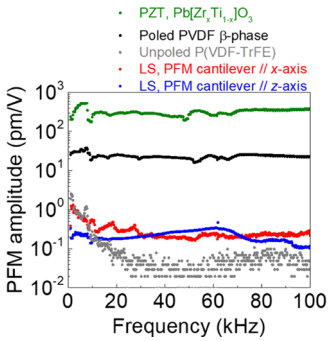

Figure 4. PFM amplitude of the LS tube as a function of frequency (1−100 kHz) in the two geometries: cantilever // the x-axis (red) and // the z-axis (blue). The out-of-plane electromechanical responses of poled PZT and PVDF β-phase and unpoled P(VDF-TrFE) are included for the comparisons. 5 V was applied to PZT, poled PVDF β-phase, and unpoled P(VDF-TrFE). The voltage applied to the LS tube was not constant since the high-voltage amplifier was used; the voltage profile as a function of frequency is included in the Supporting Information (Figure S7).

signals measured below 20 kHz are less reliable because of the acoustic noise; even from the unpoled P(VDF-TrFE) copolymer, which is non-piezoelectric, some measurable responses are observed in the 1−20 kHz region. The poled PZT and PVDF β-phase show the response around 300−400 and 20−30 pm/V, respectively, which are congruent with the reported values in the literature.[51−54] The LS tube in two different geometries shows electromechanical responses in the range of 0.1−0.3 pm/V in the 20−100 kHz region. Considering that there could be a contribution from other electrostatic effects, the intrinsic piezoelectric response would not be significantly larger than this value.

Even though the mechanism of piezoelectricity of the β-chitin crystal has not been fully addressed yet, it has long been believed that it originates from the field-induced displacement of hydrogen bonds (HBs) of hydroxyl and amine groups.[4,55] They are the main polar groups in the unit cell and have the lowest stiffness among all chemical bonds in the crystal; thus, they are the easiest to deform under the electric field.[56] Garcia et al. estimated the piezoelectric responses of individual HBs in cellulose Iβ, which is the noncentrosymmetric polysaccharide, same as chitin, to be as high as 4.3−36.4 pm/V using density functional theory (DFT).[55] However, the overall responses of a two-dimensional model of the cellulose Iβ unit cell are predicted to be much lower, 0.9−1.2 pm/V, due to the cancelation of individual responses at different angles. Also, the collective displacement of atoms to accommodate the displacements of atoms involved in the weak HBs requires physical strains in the network of C−C and C−O covalent bonds, which have extremely high stiffness (order of ∼500 N/m).[55] The same constraints should be applied to the β-chitin crystal, explaining the extremely low intrinsic piezoelectricity observed in this study, because the origin of piezoelectric responses would be the same as the cellulose Iβ structure.

3.3. Low-Frequency Regime (10^{-2}−10^{2} Hz). In a low-frequency regime, the quadratic relationship between the large strain and the electric field was observed for the LS tube, as shown in Figure 5a. Regarding the quadratic relationship, the

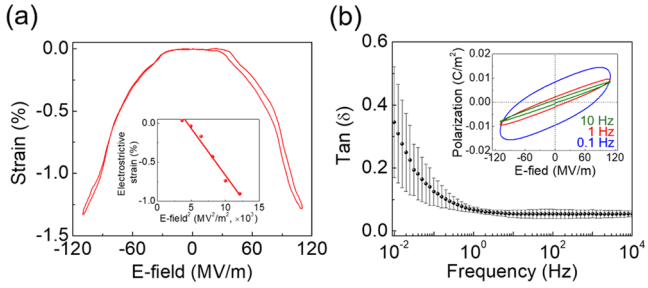

Figure 5. (a) Experimentally measured strain of the LS tube as a function of the electric field applied at 1 Hz. The electrostrictive strain (polarization-induced strain) is included in the inset. Out-of-plane measurement was performed where the applied electric field and strain are both along the z-axis of the flat LS tube, which has a thickness of 75 μm. (b) Tan(δ) as a function of frequency from 10^{-2} to 10^{4} Hz. P−E loops at 0.1, 1, and 10 Hz are included in the inset.

electrostatic and electrostrictive effects seem dominant. The electrostatic effect is induced by the Coulombic interaction of charges between the top and bottom electrodes.[57,58] Through the attractive force between the two electrodes with opposite charges, the compressive Maxwell stress can be induced across the soft LS tube.[57,58] The Maxwell stress-induced strain (S_{Maxwell}) is strongly dependent on the dielectric constant (ε_r) and Young's modulus of the material (Y)[58]

$$S_{\text{Maxwell}} = -\frac{\varepsilon_0 \varepsilon_r \cdot E^2}{Y} \tag{3}$$

where ε_0 and E are the permittivity of vacuum and the electric field applied to the system, respectively. Theoretical S_{Maxwell} of the flat LS tube was calculated with the measured dielectric constant of 16 at 1 Hz from the impedance spectrum (Section D in the Supporting Information) and Young's modulus of 458 MPa using the AFM (Section E in the Supporting Information). The calculation showed that approximately 30% of strain measured at 110 MV/m might be due to the Maxwell stress (Section D in the Supporting information). Also, the LS tube consists of noncentrosymmetric crystals surrounded by an amorphous protein matrix; thus, space charges can be induced at the interfaces between two different dielectric domains under the electric field.[59,60] The charges at the interfaces induce the strains due to the Coulombic attraction, along the same direction of the applied electric field.[59,60]

Electrostriction is a common property of any dielectric material, which is caused by the induced polarization of materials under the electric field.[61,62] Electrostrictive strain (S) can be described as a function of electrostrictive coefficient (M) and electric field (E).[61,63]

$$S_{ij} = M_{ijkl} E_k E_l \tag{4}$$

The electrostrictive strain was estimated by subtracting the Maxwell strain from the strain measured under the electric field, as shown in the inset of Figure 5a. From the linear fitting, the electrostrictive coefficient of the LS tube was measured to be -1.2×10^{-6} (m^2/MV^2). This value is in the same order of

https://doi.org/10.1021/acs.biomac.0c01799
Biomacromolecules 2021, 22, 1901−1909

magnitude as the large electrostrictive response of P(VDF-TrFE)-based co/terpolymers.[58,64,65]

The dielectric loss [tan(δ)] increases significantly in the lower-frequency regime, especially below 1 Hz, as shown in Figure 5b. Also, the $P-E$ loops (the inset of Figure 5b) show more hysteresis at 0.1 Hz than 1 Hz due to the dielectric loss. The losses in this low-frequency regime can occur due to the accumulation of charges at the interfaces, as mentioned above, and ionic migrations under the electric field. The thermal gravimetric analysis (TGA) showed approximately 4 wt % water content in the LS tube (Section F in the Supporting Information), which is enough for the extrinsic ions to move in a sample.[30]

3.4. Discussion on the Electromechanical Coupling Responses. The electromechanical coupling responses of biopolymers have been actively studied for decades due to the desirable properties of biopolymers over synthetic materials such as low density, mechanical and thermal strength, natural abundancy, and biocompatibility.[66,67] Mainly, the measured strain under the electric field (converse effect) or accumulation of charges under mechanical stress (direct effect) has been claimed or addressed as a piezoelectric effect because of the noncentrosymmetric crystalline structure of these biopolymers.[1−6,8−10] However, the exact value or mechanism at a molecular level of the intrinsic piezoelectricity originating from the noncentrosymmetric crystalline structure has not been identified yet, mainly due to the overlapping of signals originating from other electromechanical responses such as electrostriction, electrostatic, ion migration, etc.[2,3] SHG-active crystalline materials could be theoretically piezoelectric since they share the same noncentrosymmetric requirement.[18] Many studies in the past showed strong SHG responses from piezoelectric materials.[14,38,68,69] Our study demonstrates that the reverse is not necessarily true. In the case of noncentrosymmetric crystalline biopolymers, the strong SHG response does not guarantee the piezoelectricity with a measurable or meaningful magnitude. This is because of the mechanistic difference between the two processes. Piezoelectricity requires displacements of atoms locked in the crystalline lattice; it can be constrained by nonpolar covalent bonds with extremely high stiffness.[55] In contrast, SHG in the visible range requires transient displacements of electron clouds with respect to the nucleus in the crystal without the inversion symmetry, which can occur without the atomic displacements.

The LS tube with the unidirectional alignment of polar β-chitin crystals was employed in this study to test the intrinsic piezoelectricity of chitin. Piezoelectricity is usually measured across the entire sample; thus, the distance between two electrodes of the sample is equivalent to the coherence length of the measurement. The piezoelectric responses of individual domains between the two electrodes can be added or canceled depending on their relative orientations; without ensuring the polar ordering of all domains, the addition of the piezoelectric responses of individual domains cannot be guaranteed.[36] In ferroelectric materials, such macroscopic polar ordering across the entire sample can be induced by applying the electric field above the coercive field.[25,70] However, most biomaterials containing noncentrosymmetric crystals including β-chitin and cellulose Iβ are not ferroelectric; in other words, the orientation of crystal polarity cannot be rearranged by simply applying an external electric field. The $P-E$ loop of the LS tube (Figure 5b) shows some degree of "remnant" polarization at a zero electric field at lower frequencies in the 0.1−10 Hz regime. However, this is due to the lossy behavior of the dielectric property and not due to the alignment of polar domains. In other words, the hysteresis appears due to the dielectric loss and not due to the flipping of dipoles in the crystalline domains.[71]

The investigated LS tube naturally has the polar packing of β-chitin crystals in the entire sample (see Figure S2 in the Supporting Information).[16] Therefore, the intrinsic piezoelectric responses of individual crystalline domains between the two electrodes could be added to an experimentally measurable value. Our investigation shows that the intrinsic piezoelectricity of the LS tube, which represents polar β-chitin crystals, has very weak piezoelectricity, in the order of ∼0.3 pm/V at maximum. Although the piezoelectric responses of individual hydrogen bonds could be large, their collective response across the entire crystal appears to be quite small due to the cancelation among bonds pointing to different orientations and the stiffness of other covalent bonds, as suggested in the recent computational study.[55] One might think that the small response should be due to a restriction from surrounding protein matrices, but considering the high concentration of β-chitin crystals in the LS tube (∼50 wt %)[16,72] and the deformability of the matrix between β-chitin crystals, as shown in Figure 5b, the actual piezoelectric response of the β-chitin crystal is only in the vicinity of ∼0.3 pm/V at best.

4. CONCLUSIONS

The polarization responses of the LS tube, which has unidirectionally aligned β-chitin crystals, were experimentally investigated in different frequency domains, and their mechanisms were elucidated. In the optical frequency regime, the large nonlinear polarization along the long axis of the tube was induced with the oscillations of electron clouds by the incidence of the polarized light. In the acoustic/ultrasonic frequency regime, the weak piezoelectric response was measured as atomic displacements occur under the electric field. In the low-frequency regime, strong electrostriction and electrostatic strains were observed due to the accumulation of charges at the interfaces. It is very important to differentiate the polarization mechanisms in different frequency regimes and apply the right concept to utilize the noncentrosymmetric biopolymers accurately.

■ ASSOCIATED CONTENT

Supporting Information

The Supporting Information is available free of charge at https://pubs.acs.org/doi/10.1021/acs.biomac.0c01799.

Details of SHG fitting; comparison of PFM signals of curved and flat LS tubes; high-voltage profile as a function of frequency in the PFM measurement; Young's modulus measurement; and calculation of the Maxwell stress-induced strain and TGA analysis of the LS tube (PDF)

■ AUTHOR INFORMATION

Corresponding Author

Seong H. Kim − *Department of Chemical Engineering and Materials Research Institute, Pennsylvania State University, University Park, Pennsylvania 16802, United States;*

https://doi.org/10.1021/acs.biomac.0c01799
Biomacromolecules 2021, 22, 1901−1909

orcid.org/0000-0002-8575-7269; Email: shkim@engr.psu.edu, shk10@psu.edu

Authors

Inseok Chae − *Department of Chemical Engineering and Materials Research Institute, Pennsylvania State University, University Park, Pennsylvania 16802, United States*

Rui Zu − *Department of Materials Science and Engineering, Pennsylvania State University, University Park, Pennsylvania 16802, United States;* orcid.org/0000-0002-9944-4757

Amira Barhoumi Meddeb − *Department of Mechanical Engineering and Materials Research Institute, Pennsylvania State University, University Park, Pennsylvania 16802, United States*

Yu Ogawa − *Univ. Grenoble Alpes, CNRS, CERMAV, 38000 Grenoble, France;* orcid.org/0000-0003-0677-7913

Zhe Chen − *Department of Chemical Engineering and Materials Research Institute, Pennsylvania State University, University Park, Pennsylvania 16802, United States;* orcid.org/0000-0002-5874-7196

Venkatraman Gopalan − *Department of Materials Science and Engineering, Department of Physics, and Department of Engineering Science and Mechanics, Pennsylvania State University, University Park, Pennsylvania 16802, United States;* orcid.org/0000-0001-6866-3677

Zoubeida Ounaies − *Department of Mechanical Engineering and Materials Research Institute, Pennsylvania State University, University Park, Pennsylvania 16802, United States*

Complete contact information is available at: https://pubs.acs.org/10.1021/acs.biomac.0c01799

Notes

The authors declare no competing financial interest.

■ ACKNOWLEDGMENTS

This work was supported by the iSuperSEED program of the Penn State Materials Research Science & Engineering Center funded by the National Science Foundation, NSF (Grant No. DMR-1420620). The SHG measurement work was supported by another NSF program (Grant No. DMR-1807768). Yu Ogawa thanks Dr. Hiroshi Miyake and the Japan Agency for Marine-Earth Science and Technology (JAMSTEC) for collecting samples of Lamellibrachia satsuma using the remotely operated vehicle, Hyper-Dolphin.

■ REFERENCES

(1) Fukada, E. Piezoelectricity in polymers and biological materials. *Ultrasonics* **1968**, *6*, 229−234.

(2) Chae, I.; Jeong, C. K.; Ounaies, Z.; Kim, S. H. Review on Electromechanical Coupling Properties of Biomaterials. *ACS Appl. Bio Mater.* **2018**, *1*, 936−953.

(3) Guerin, S.; Tofail, S. A. M.; Thompson, D. Organic piezoelectric materials: milestones and potential. *NPG Asia Mater.* **2019**, *11*, No. 10.

(4) Fukada, E.; Yasuda, I. Piezoelectric Effects in Collagen. *Jpn. J. Appl. Phys.* **1964**, *3*, 117−121.

(5) Fukada, E. Piezoelectric properties of biological polymers. *Q. Rev. Biophys.* **1983**, *16*, 59−87.

(6) Rajala, S.; Siponkoski, T.; Sarlin, E.; Mettänen, M.; Vuoriluoto, M.; Pammo, A.; Juuti, J.; Rojas, O. J.; Franssila, S.; Tuukkanen, S. Cellulose Nanofibril Film as a Piezoelectric Sensor Material. *ACS Appl. Mater. Interfaces* **2016**, *8*, 15607−15614.

(7) Lee, B. Y.; Zhang, J.; Zueger, C.; Chung, W.-J.; Yoo, S. Y.; Wang, E.; Meyer, J.; Ramesh, R.; Lee, S.-W. Virus-based piezoelectric energy generation. *Nat. Nanotechnol.* **2012**, *7*, 351−356.

(8) Kim, J.; Yun, S.; Ounaies, Z. Discovery of Cellulose as a Smart Material. *Macromolecules* **2006**, *39*, 5583.

(9) Li, T.; Zeng, K. Nanoscale piezoelectric and ferroelectric behaviors of seashell by piezoresponse force microscopy. *J. Appl. Phys.* **2013**, *113*, No. 187202.

(10) Kim, K.; Ha, M.; Choi, B.; Joo, S. H.; Kang, H. S.; Park, J. H.; Gu, B.; Park, C.; Park, C.; Kim, J.; Kwak, S. K.; Ko, H.; Jin, J.; Kang, S. J. Biodegradable, electro-active chitin nanofiber films for flexible piezoelectric transducers. *Nano Energy* **2018**, *48*, 275−283.

(11) Yun, G.-Y.; Kim, J.-H.; Kim, J. Dielectric and polarization behaviour of cellulose electro-active paper (EAPap). *J. Phys. D: Appl. Phys.* **2009**, *42*, No. 082003.

(12) Frka-Petesic, B.; Jean, B.; Heux, L. First experimental evidence of a giant permanent electric-dipole moment in cellulose nanocrystals. *EPL* **2014**, *107*, No. 28006.

(13) Gindl, W.; Emsenhuber, G.; Maier, G.; Keckes, J. Cellulose in Never-Dried Gel Oriented by an AC Electric Field. *Biomacromolecules* **2009**, *10*, 1315−1318.

(14) Lee, J.-H.; Lee, J. H.; Xiao, J.; Desai, M. S.; Zhang, X.; Lee, S.-W. Vertical Self-Assembly of Polarized Phage Nanostructure for Energy Harvesting. *Nano Lett.* **2019**, *19*, 2661−2667.

(15) Zugenmaier, P. Cellulose. In *Crystalline Cellulose and Derivatives: Characterization and Structures*; Springer Berlin Heidelberg: Berlin, Heidelberg, 2008; pp 101−174.

(16) Ogawa, Y.; Kobayashi, K.; Kimura, S.; Nishiyama, Y.; Wada, M.; Kuga, S. X-ray texture analysis indicates downward spinning of chitin microfibrils in tubeworm tube. *J. Struct. Biol.* **2013**, *184*, 212−216.

(17) Kobayashi, K.; Kimura, S.; Togawa, E.; Wada, M. Crystal transition between hydrate and anhydrous β-chitin monitored by synchrotron X-ray fiber diffraction. *Carbohydr. Polym.* **2010**, *79*, 882−889.

(18) Halasyamani, P. S.; Poeppelmeier, K. R. Noncentrosymmetric Oxides. *Chem. Mater.* **1998**, *10*, 2753−2769.

(19) Street, R. M.; Huseynova, T.; Xu, X.; Chandrasekaran, P.; Han, L.; Shih, W. Y.; Shih, W.-H.; Schauer, C. L. Variable piezoelectricity of electrospun chitin. *Carbohydr. Polym.* **2018**, *195*, 218−224.

(20) Hänninen, A.; Sarlin, E.; Lyyra, I.; Salpavaara, T.; Kellomäki, M.; Tuukkanen, S. Nanocellulose and chitosan based films as low cost, green piezoelectric materials. *Carbohydr. Polym.* **2018**, *202*, 418−424.

(21) Tayeb, P.; H. Tayeb, A. Nanocellulose applications in sustainable electrochemical and piezoelectric systems: A review. *Carbohydr. Polym.* **2019**, *224*, No. 115149.

(22) Zhu, Q.; Liu, S.; Sun, J.; Liu, J.; Kirubaharan, C. J.; Chen, H.; Xu, W.; Wang, Q. Stimuli-responsive cellulose nanomaterials for smart applications. *Carbohydr. Polym.* **2020**, *235*, No. 115933.

(23) Ogawa, Y.; Lee, C. M.; Nishiyama, Y.; Kim, S. H. Absence of Sum Frequency Generation in Support of Orthorhombic Symmetry of α-Chitin. *Macromolecules* **2016**, *49*, 7025−7031.

(24) Chae, I.; Ngo, D.; Makarem, M.; Ounaies, Z.; Kim, S. H. Compression-Induced Topographic Corrugation of Air/Surfactant/Water Interface: Effect of Nanoparticles Adsorbed beneath the Interface. *J. Phys. Chem. C* **2019**, *123*, 25628−25634.

(25) Chae, I.; Ahmed, S.; Atitallah, H. B.; Luo, J.; Wang, Q.; Ounaies, Z.; Kim, S. H. Vibrational Sum Frequency Generation (SFG) Analysis of Ferroelectric Response of PVDF-Based Copolymer and Terpolymer. *Macromolecules* **2017**, *50*, 2838−2844.

(26) Chae, I.; Ngo, D.; Chen, Z.; Kwansa, A. L.; Chen, X.; Meddeb, A. B.; Podraza, N. J.; Yingling, Y. G.; Ounaies, Z.; Kim, S. H. Anisotropic Optical and Frictional Properties of Langmuir−Blodgett Film Consisting of Uniaxially-Aligned Rod-Shaped Cellulose Nanocrystals. *Adv. Mater. Interfaces* **2020**, *7*, No. 1902169.

(27) Chae, I.; Bokhari, S. M. Q.; Chen, X.; Zu, R.; Liu, K.; Borhan, A.; Gopalan, V.; Catchmark, J. M.; Kim, S. H. Shear-induced

unidirectional deposition of bacterial cellulose microfibrils using rising bubble stream cultivation. *Carbohydr. Polym.* **2021**, *255*, No. 117328.
(28) Makarem, M.; Lee, C. M.; Kafle, K.; Huang, S.; Chae, I.; Yang, H.; Kubicki, J. D.; Kim, S. H. Probing cellulose structures with vibrational spectroscopy. *Cellulose* **2019**, *26*, 35−79.
(29) Meddeb, A. B.; Chae, I.; Scurti, F.; Schwartz, J.; Kim, S. H.; Ounaies, Z. From a cholesteric non-aqueous cellulose nanocrystal suspension to a highly ordered film. *MRS Adv.* **2020**, *5*, 3547−3554.
(30) Nayak, J. N.; Chen, Y.; Yun, S.; Kim, J. Effect of Li+ ions on structure, properties, and actuation of cellulose electro-active paper actuator. *J. Appl. Polym. Sci.* **2008**, *108*, 2260−2265.
(31) Shahid UN, M.; Deshpande, A. P.; Rao, C. L. Electro-mechanical properties of hydrogel composites with micro- and nano-cellulose fillers. *Smart Mater. Struct.* **2015**, *24*, No. 095013.
(32) Newnham, R. E. *Properties of Materials Anisotropy, Symmetry, Structure*; Oxford University Press: New York, 2005.
(33) Dorey, R. Microstructure−Property Relationships: How the Microstructure of the Film Affects Its Properties. In *Ceramic Thick Films for MEMS and Microdevices*; Dorey, R., Ed.; William Andrew Publishing: Oxford, 2012; Chapter 4, pp 85−112.
(34) Kim, S.; Choi, S. J.; Zhao, K.; Yang, H.; Gobbi, G.; Zhang, S.; Li, J. Electrochemically driven mechanical energy harvesting. *Nat. Commun.* **2016**, *7*, No. 10146.
(35) Thurmond, F. A.; Trotter, J. A. Native collagen fibrils from echinoderms are molecularly bipolar. *J. Mol. Biol.* **1994**, *235*, 73−79.
(36) Trolier-McKinstry, S. Crystal Chemistry of Piezoelectric Materials. In *Piezoelectric and Acoustic Materials for Transducer Applications*; Safari, A.; Akdoğan, E. K., Eds.; Springer US: Boston, MA, 2008; pp 39−56.
(37) Lee, C. M.; Kafle, K.; Park, Y. B.; Kim, S. H. Probing crystal structure and mesoscale assembly of cellulose microfibrils in plant cell walls, tunicate tests, and bacterial films using vibrational Sum Frequency Generation (SFG) spectroscopy. *Phys. Chem. Chem. Phys.* **2014**, *16*, 10844−10853.
(38) Denev, S. A.; Lummen, T. T. A.; Barnes, E.; Kumar, A.; Gopalan, V. Probing Ferroelectrics Using Optical Second Harmonic Generation. *J. Am. Ceram. Soc.* **2011**, *94*, 2699−2727.
(39) Mohebbi, A.; Mighri, F.; Ajji, A.; Rodrigue, D. Cellular Polymer Ferroelectret: A Review on Their Development and Their Piezo-electric Properties. *Adv. Polym. Technol.* **2018**, *37*, 468−483.
(40) Newnham, R. E. *Properties of Materials Anisotropy, Symmetry, Structure*; Oxford University Press: New York, 2005.
(41) Gopalan, V.; Raj, R. Domain structure and phase transitions in epitaxial KNbO3 thin films studied by in situ second harmonic generation measurements. *Appl. Phys. Lett.* **1996**, *68*, 1323−1325.
(42) Kim, T. H.; Puggioni, D.; Yuan, Y.; Xie, L.; Zhou, H.; Campbell, N.; Ryan, P. J.; Choi, Y.; Kim, J. W.; Patzner, J. R.; Ryu, S.; Podkaminer, J. P.; Irwin, J.; Ma, Y.; Fennie, C. J.; Rzchowski, M. S.; Pan, X. Q.; Gopalan, V.; Rondinelli, J. M.; Eom, C. B. Polar metals by geometric design. *Nature* **2016**, *533*, 68−72.
(43) "IEEE Standard on Piezoelectricity," in *ANSI/IEEE Std 176-1987*, 1988.
(44) Seol, D.; Kim, B.; Kim, Y. Non-piezoelectric effects in piezoresponse force microscopy. *Curr. Appl. Phys.* **2017**, *17*, 661−674.
(45) Kim, S.; Seol, D.; Lu, X.; Alexe, M.; Kim, Y. Electrostatic-free piezoresponse force microscopy. *Sci. Rep.* **2017**, *7*, No. 41657.
(46) Nguyen, T. D.; Mao, S.; Yeh, Y.-W.; Purohit, P. K.; McAlpine, M. C. Nanoscale Flexoelectricity. *Adv. Mater.* **2013**, *25*, 946−974.
(47) Vasudevan, R. K.; Balke, N.; Maksymovych, P.; Jesse, S.; Kalinin, S. V. Ferroelectric or non-ferroelectric: Why so many materials exhibit "ferroelectricity" on the nanoscale. *Appl. Phys. Rev.* **2017**, *4*, No. 021302.
(48) Kalinin, S. V.; Rodriguez, B. J.; Jesse, S.; Shin, J.; Baddorf, A. P.; Gupta, P.; Jain, H.; Williams, D. B.; Gruverman, A. Vector Piezoresponse Force Microscopy. *Microsc. Microanal.* **2006**, *12*, 206−220.
(49) Harnagea, C.; Vallières, M.; Pfeffer, C. P.; Wu, D.; Olsen, B. R.; Pignolet, A.; Légaré, F.; Gruverman, A. Two-dimensional nanoscale structural and functional imaging in individual collagen type I fibrils. *Biophys. J.* **2010**, *98*, 3070−3077.
(50) Nath, R.; Hong, S.; Klug, J. A.; Imre, A.; Bedzyk, M. J.; Katiyar, R. S.; Auciello, O. Effects of cantilever buckling on vector piezoresponse force microscopy imaging of ferroelectric domains in BiFeO3 nanostructures. *Appl. Phys. Lett.* **2010**, *96*, No. 163101.
(51) Erhart, J. Experiments to demonstrate piezoelectric and pyroelectric effects. *Phys. Educ.* **2013**, *48*, 438−447.
(52) Sirohi, J.; Chopra, I. Fundamental Understanding of Piezo-electric Strain Sensors. *J. Intell. Mater. Syst. Struct.* **2000**, *11*, 246−257.
(53) Dekkers, M.; Boschker, H.; Zalk, Mv.; Nguyen, M.; Nazeer, H.; Houwman, E.; Rijnders, G. The significance of the piezoelectric coefficient d 31,eff determined from cantilever structures. *J. Micromech. Microeng.* **2013**, *23*, No. 025008.
(54) Moheimani, S. O. R.; Fleming, J. A. Fundamentals of Piezoelectricity. In *Piezoelectric Transducers for Vibration Control and Damping*; Springer London: London, 2006; pp 9−35.
(55) García, Y.; Ruiz-Blanco, Y. B.; Marrero-Ponce, Y.; Sotomayor-Torres, C. M. Orthotropic Piezoelectricity in 2D Nanocellulose. *Sci. Rep.* **2016**, *6*, No. 34616.
(56) Werling, K. A.; Griffin, M.; Hutchison, G. R.; Lambrecht, D. S. Piezoelectric Hydrogen Bonding: Computational Screening for a Design Rationale. *J. Phys. Chem. A* **2014**, *118*, 7404−7410.
(57) Kloos, G. *Maxwell Stresses and Dielectric Materials*; Trans Tech Publications Limited, 2008.
(58) Qiao, B.; Wang, X.; Tan, S.; Zhu, W.; Zhang, Z. Synergistic Effects of Maxwell Stress and Electrostriction in Electromechanical Properties of Poly(vinylidene fluoride)-Based Ferroelectric Polymers. *Macromolecules* **2019**, *52*, 9000−9011.
(59) Wegener, M.; Bauer, S. Microstorms in Cellular Polymers: A Route to Soft Piezoelectric Transducer Materials with Engineered Macroscopic Dipoles. *ChemPhysChem* **2005**, *6*, 1014−1025.
(60) Neugschwandtner, G. S.; Schwödiauer, R.; Bauer-Gogonea, S.; Bauer, S. Large piezoelectric effects in charged, heterogeneous fluoropolymer electrets. *Appl. Phys. A: Mater. Sci. Process.* **2000**, *70*, 1−4.
(61) Sundar, V.; Newnham, R. E. Electrostriction and polarization. *Ferroelectrics* **1992**, *135*, 431−446.
(62) Li, F.; Jin, L.; Xu, Z.; Zhang, S. Electrostrictive effect in ferroelectrics: An alternative approach to improve piezoelectricity. *Appl. Phys. Rev.* **2014**, *1*, No. 011103.
(63) Newnham, R. E.; Sundar, V.; Yimnirun, R.; Su, J.; Zhang, Q. M. Electrostriction: Nonlinear Electromechanical Coupling in Solid Dielectrics. *J. Phys. Chem. B* **1997**, *101*, 10141−10150.
(64) Cheng, Z.-Y.; Xu, H.; Mai, T.; Chung, T. C. M.; Zhang, Q. M.; Ting, R. P(DF-TrFE)-based electrostrictive co/terpolymers and their device performance. *Proc. SPIE* **2001**, *4329*, 106−116.
(65) Zhang, Q. M.; Bharti, V.; Zhao, X. Giant Electrostriction and Relaxor Ferroelectric Behavior in Electron-Irradiated Poly(vinylidene fluoride-trifluoroethylene) Copolymer. *Science* **1998**, *280*, 2101−2104.
(66) Ribeiro, C.; Sencadas, V.; Correia, D. M.; Lanceros-Méndez, S. Piezoelectric polymers as biomaterials for tissue engineering applications. *Colloids Surf., B* **2015**, *136*, 46−55.
(67) Li, J.; Long, Y.; Yang, F.; Wang, X. Degradable piezoelectric biomaterials for wearable and implantable bioelectronics. *Curr. Opin. Solid State Mater. Sci.* **2020**, *24*, No. 100806.
(68) Miller, R. C. Optical Second Harmonic Generation in Piezoelectric Crystals. *Appl. Phys. Lett.* **1964**, *5*, 17−19.
(69) Xue, F.; Zhang, J.; Hu, W.; Hsu, W.-T.; Han, A.; Leung, S.-F.; Huang, J.-K.; Wan, Y.; Liu, S.; Zhang, J.; He, J.-H.; Chang, W.-H.; Wang, Z. L.; Zhang, X.; Li, L.-J. Multidirection Piezoelectricity in Mono- and Multilayered Hexagonal α-In2Se3. *ACS Nano* **2018**, *12*, 4976−4983.
(70) Lovinger, A. J. Ferroelectric Polymers. *Science* **1983**, *220*, 1115−1121.
(71) Scott, J. F. Ferroelectrics go bananas. *J. Phys.: Condens. Matter* **2007**, *20*, No. 021001.

https://doi.org/10.1021/acs.biomac.0c01799
Biomacromolecules 2021, 22, 1901−1909

(72) Gaill, F.; Persson, J.; Sugiyama, J.; Vuong, R.; Chanzy, H. The chitin system in the tubes of deep sea hydrothermal vent worms. *J. Struct. Biol.* **1992**, *109*, 116−128.

https://doi.org/10.1021/acs.biomac.0c01799
Biomacromolecules 2021, 22, 1901−1909